ingegneria sismica
International Journal of Earthquake Engineering
Anno XLIII - Num. 1 - 2026

Mathematical Modeling Method for the Optimal Power Flow Problem of Power Systems under Multi-norm Constraints

Maolin Sheng[1,*]

[1] Department of Basic Education, Anhui Electrical Engineering Professional Technique College, 230051, Anhui, China

SUMMARY: *This paper addresses the difficulty of traditional optimal power flow (OPF) models in high-renewable active distribution networks, where it is hard to simultaneously control overall voltage deviation, local limit violations and a few abnormal points. A distributed OPF model with multi-norm constraints is formulated by expressing voltage deviations, line loading rates and distributed generation outputs as deviation vectors and constraining them in a multi-scenario framework. An ADMM-based region–scenario decomposition is adopted for scalable solution. Case studies on modified IEEE 33-bus (DG 3.0 MW, storage 1.0 MW, maximum load 3.7 MW) and 69-bus systems (DG 5.5 MW, storage 2.0 MW, maximum load 5.8 MW) with 20 representative scenarios show that, under a 2-norm voltage deviation limit of 0.08 p.u. and an infinity-norm limit of 0.05 p.u., the multi-norm scheme suppresses long-tail voltage deviations at terminal buses and smooths normalized performance curves while maintaining network security and economic efficiency.*

Povzetek: This paper develops a distributed OPF model with multi-norm constraints for high-renewable active distribution networks. Voltage deviations, line loading rates and distributed generation outputs are aggregated into deviation vectors and constrained by combined 2-norm and infinity-norm limits within a 20-scenario framework. Tests on modified IEEE 33-bus (DG 3.0 MW, storage 1.0 MW, max load 3.7 MW) and 69-bus systems (DG 5.5 MW, storage 2.0 MW, max load 5.8 MW) under 0.08 p.u. (2-norm) and 0.05 p.u. (∞-norm) voltage-deviation thresholds show that the method suppresses long-tail voltage deviations, smooths normalized performance indices and maintains secure, economical operation.

KEYWORDS: *Multi-norm constraints; Optimal power flow; Distributed solution*

1 Introduction

Optimal Power Flow (OPF) is a fundamental issue in power system operation and dispatch. It has long been used to optimize costs and network losses while satisfying power flow equations and safety constraints. In recent years, Lei Zhang [3] has integrated OPF with economic dispatch through the introduction of various intelligent optimization algorithms, significantly improving the solution efficiency in large-scale systems. However, his research focuses more on algorithm performance improvement and has relatively limited detailed description of multi-scenario operational risks. Priya E. and Preetha Roselyn [7] combined multi-objective differential evolution algorithms with event constraints to incorporate resilience and fault scenarios into the OPF framework, which is beneficial for enhancing the system's anti-disturbance capability. However, their approach mainly compares "before/after events" and

*qifuxyslwm2668@126.com
https://doi.org/10.65102/is2026094
Published: 30 April, 2026

pays less attention to continuous deviation control during daily multi-scenario fluctuations. Mokhtar Abid et al. [15] used the improved Kepler algorithm to solve OPF on a large-scale actual thermal-fuel-power system, verifying the feasibility of intelligent optimization in engineering examples. However, their model still mainly relies on traditional safety constraints and a single deviation metric, lacking specific characterization of phenomena such as "long-tail low voltage" at the end. Saeed Badoozadeh et al. [17] used probabilistic OPF and K-medoids clustering to handle wind power uncertainties, reflecting the impact of source-load fluctuations on the optimal power flow from a statistical distribution perspective. However, their focus is on modeling probability distributions and correlations, and does not make a detailed distinction between "overall deviation, extreme deviation, and cumulative effects of scenarios". Nguyen Thang Trung et al. [20] incorporated the power market, electricity price signals, and renewable output into OPF, analyzing the operational optimization problem under market mechanisms, emphasizing the coupling of economic incentives and power flow, while paying limited attention to the fine constraints of multi-scenario voltage quality and line load distribution at the distribution network side.

Overall, these works have made significant progress in intelligent solution, uncertainty modeling, and multi-objective trade-offs. However, most of them are still based on a single two-norm objective or traditional safety constraints, evaluating operational quality from an "average perspective" or based on a few representative scenarios. They are unable to simultaneously characterize overall voltage deviations, single-node extreme over-limit conditions, and cumulative effects of a few abnormal scenarios in active distribution network multi-scenario operations. To address this deficiency, this paper focuses on active distribution networks with distributed power sources and energy storage. In the multi-scenario OPF framework, it introduces a multi-norm combination, uniformly representing node voltage deviations and line load rate deviations as deviation vectors. It simultaneously constrains overall deviation, maximum deviation, and cross-scenario cumulative deviation within the same model. By combining a mathematical form that can be transformed into cone constraints with a distributed solution strategy, it constructs a modeling method for the optimal power flow under multi-norm constraints, providing support for subsequent multi-scenario operation analysis and parameter tuning under "safety-economy" trade-offs in active distribution networks.

2 Description of the Optimal Power Flow Problem in Power Systems under Multi-norm Constraints

The basic task of the Optimal Power Flow (OPF) in power systems is to optimize the configuration of control variables such as the output of distributed power sources, the charging and discharging power of energy storage devices, node voltages, and adjustable load levels, under the condition of satisfying the power flow equations and various operational constraints, so as to achieve the unified goal of "safety and feasibility" and "economy and rationality" for the system under given operating conditions. Traditional OPF models usually aim to minimize fuel costs or network losses, and the constraint forms mainly include power balance equations, generator output upper and lower limits, node voltage ranges, and branch power flow limits, etc. Their basic form can be summarized as:

$$\min f(x)\ s.t.\ g(x) = 0, h(x) \le 0 \tag{1}$$

Among them, x is the decision variable vector, $f(x)$ represents the optimization objective, $g(x) = 0$ is the power balance constraint, and $h(x) \leq 0$ is the various inequality operational constraints. In recent years, a large number of works related to this framework have emerged, such as solving multi-objective OPF using swarm intelligence algorithms or expanding the OPF model in scenarios with uncertainties of renewable energy, multi-regional coupling, and stability constraints [1], [4], [14].

In traditional AC-OPF, the decision variables are generally written as:

$$\mathrm{x} = [\mathrm{P_G}, \mathrm{Q_G}, \mathrm{V}, \theta]^{\mathrm{T}} \tag{2}$$

Among them, PG, QG are the active and reactive power output vectors of the units, V, θ are the amplitude and phase angle of each node voltage. For each node $\mathrm{i} \in \mathrm{N}$ (N is the set of nodes), the active and reactive balance constraints can be written as:

$$\begin{cases} \mathrm{P_i}(\mathrm{V}, \theta) - \mathrm{P_{D,i}} = 0 \\ (\mathrm{V}, \theta) - \mathrm{Q_{D,i}} = 0 \end{cases} \tag{3}$$

Among them, $\mathrm{P_{D,i}}$, $\mathrm{Q_{D,i}}$ are the load. The operational constraints include the upper and lower limits of generator output, node voltage, and branch power flow:

$$\begin{aligned} &\mathrm{P_G^{min}} \leq \mathrm{P_G} \leq \mathrm{P_G^{max}}, \quad \mathrm{Q_G^{min}} \leq \mathrm{Q_G} \leq \mathrm{Q_G^{max}}, \\ &\mathrm{V^{min}} \leq \mathrm{V} \leq \mathrm{V^{max}}, \\ &|\mathrm{S_{ij}}(\mathrm{V}, \theta)| \leq \mathrm{S_{ij}^{max}}, \quad (\mathrm{i}, \mathrm{j}) \in \mathcal{L}, \end{aligned} \tag{4}$$

Among them, L is the set of branches, $\mathrm{S_{ij}}$ is the branch power flow. Formulas (3)–(4) constitute the basic constraint framework of OPF.

With the large-scale integration of renewable energy sources such as wind power and photovoltaic power, as well as the intensification of load fluctuations, the operating state of the system exhibits characteristics such as "significant overall deviation, sensitive local over-limit, and amplified influence of a few abnormal points". Many studies have introduced safety constraints, probabilistic constraints, or scenario-based constraints on the basis of traditional constraints to better reflect the uncertainty of renewable power output and load on OPF [2]. However, these constraints are still mostly expressed using a single norm or point-wise intervals, making it difficult to simultaneously depict the operating state from multiple perspectives such as "overall level", "worst-case scenario", and "sparse anomalies".

The introduction of multi-norm constraints is precisely to address this issue. In the power grid, a certain type of operating deviation quantity (such as node voltage deviation, line load rate deviation, multi-period power flow deviation, etc.) can be composed into a vector:

$$\mathrm{z}(\mathrm{x}) \in \mathbb{R}^{\mathrm{n}} \tag{5}$$

and multiple norm constraints can be imposed on it in the same model. For example, for the node voltage deviation vector $\mathrm{z_V}(\mathrm{x})$, it can be simultaneously constrained by its 2-norm and infinity norm:

$$\|\mathrm{z_V}(\mathrm{x})\|_2 \leq \gamma_2, \quad \|\mathrm{z_V}(\mathrm{x})\|_\infty \leq \gamma_\infty \tag{6}$$

The 2-norm reflects the overall deviation level, while the infinity norm limits the maximum over-limit amplitude of a single node. For the branch power flow deviation vector $z_S(x)$ in multi-period or multi-scenario, a 1-norm can also be introduced:

$$\|z_S(x)\|_1 \leq \gamma_1 \tag{7}$$

To emphasize the control of "a few severely overloaded branches", the system resilience requirement is introduced mathematically into the model.

Combining the above constraints, the OPF problem under multi-norm constraints can be expressed as:

$$\begin{aligned} \min f(x) \quad & s.t.\, g(x) = 0, h(x) \leq 0, \\ & \|z_k(x)\|_{p_k} \leq \gamma_k, k = 1, \ldots, K \end{aligned} \tag{8}$$

Among them, $z_k(x)$ is the deviation vector of the kth type, $p_k \in \{1, 2, \infty\}$ is the corresponding norm type, γ_k is the given threshold, and K is the total number of multi-norm constraints. Compared with traditional OPF that only uses a single norm or simple interval constraints, equations (5-8) simultaneously depict the overall deviation, local extremum, and sparse anomalies in a unified framework, providing a foundation for constructing a more refined optimal power flow model in power systems with large-scale renewable energy integration, multi-regional interconnection, and multi-scenario operation [5].

It can be seen that multi-norm constraints not only increase the number of constraints but also change the mathematical structure of the OPF problem: L_1 and L_∞ constraints introduce non-smooth characteristics, and there may also be coupling relationships among multiple norms, affecting the shape of the feasible region and the properties of the optimal solution. These changes make traditional modeling and analysis methods based on the assumption of a single norm difficult to directly apply, and also bring new challenges to the design of subsequent mathematical modeling methods [6]. Based on the unified description given in this section, the following will focus on "how to construct the mathematical model of OPF under multi-norm constraints" for specific modeling discussions.

3 Mathematical Modeling Method for Optimal Power Flow of Power System under Multi-norm Constraints

3.1 The extended form of the optimal power flow in the power system

To adapt to multiple scenarios (or multiple time periods) of operation conditions and provide a carrier for the unified depiction of multiple-norm constraints in the future, this paper expands the optimal power flow model from a single condition to a joint form over a set of scenarios. Let $\Omega = \{1, \ldots, N_\Omega\}$ be the set of scenarios, and $\omega \in \Omega$ represent the ωth operation scenario. For each scenario, introduce the decision variable vector:

$$x^{(\omega)} = [P_G^{(\omega)}, Q_G^{(\omega)}, V^{(\omega)}, \theta^{(\omega)}]^T, \omega \in \Omega \tag{9}$$

Consider the weights πω for each scenario, and aggregate the operation objectives in the scenario set with weights, obtaining the form of the multi-scenario extended objective function:

$$\min_{\{x^{(\omega)}\}} \sum_{\omega \in \Omega} \pi_\omega \, f\left(x^{(\omega)}\right) \tag{10}$$

Under this extended framework, each scenario still needs to satisfy the corresponding physical feasibility and operation restrictions.

To apply multi-norm constraints to the operation deviation quantities with clear physical meanings, define the mapping of the kth type deviation vector under scenario ω as

$$z_k^{(\omega)} = \psi_k^{(\omega)}\left(x^{(\omega)}\right), \omega \in \Omega, k = 1, \ldots, K \tag{11}$$

Among them, $\psi_k^{(\omega)}(\cdot)$ is the deviation mapping function. Further, concatenate the deviation vectors of each scenario in sequence to construct a unified deviation vector:

$$\bar{z_k} = \begin{bmatrix} z_k^{(1)} \\ z_k^{(2)} \\ \vdots \\ z_k^{(N_\Omega)} \end{bmatrix} \in \mathbb{R}^{n_k N_\Omega} \tag{12}$$

Accordingly, the model after the multi-scenario extension can be represented in a more compact form as:

$$\min_{\{x^{(\omega)}\}} \sum_{\omega \in \Omega} \pi_\omega \, f\left(x^{(\omega)}\right) \quad \text{s.t.} \quad \bar{z_k} \in \mathcal{Z}_k, k = 1, \ldots, K \tag{13}$$

Among them, $\mathcal{Z}_k$ is the feasible set of the kth type deviation vector. In the next section, the multi-norm constraint expressions of $\mathcal{Z}_k$ will be given to control the deviation simultaneously at different scales.

3.2 The mathematical expression and formalization of multi-norm constraints

To simultaneously depict the overall deviation, local extremum, and cumulative deviation in the same optimal power flow model, the key operating quantities are expressed as deviation vectors, and multiple norm constraints are imposed on them [8]. Let the scenario set be $\Omega = \{1, \ldots, N_\Omega\}$, and define the deviation mapping for the k-th type of operating indicator as:

$$z_k^{(\omega)} = \psi_k^{(\omega)}\left(x^{(\omega)}\right), \omega \in \Omega \tag{14}$$

And the unified deviation vector is obtained by concatenating scenarios:

$$\bar{z_k} = \begin{bmatrix} z_k^{(1)} \\ z_k^{(2)} \\ \vdots \\ z_k^{(N_\Omega)} \end{bmatrix} \tag{15}$$

Given threshold values $\gamma_{k,1}, \gamma_{k,2}, \gamma_{k,\infty} > 0$, the multiple norm constraints can be written as:

$$\begin{aligned} &\|\bar{z_k}\|_1 \le \gamma_{k,1}, \quad \|\bar{z_k}\|_2 \le \gamma_{k,2}, \\ &\|\bar{z_k}\|_\infty \le \gamma_{k,\infty}, k = 1, \ldots, K \end{aligned} \tag{16}$$

Among them, $\|\bar{z_k}\|_2$ is the constraint on the overall deviation level, $\|\bar{z_k}\|_\infty$ is the control of the maximum component's local over-limit risk, and $\|\bar{z_k}\|_1$ is then used to depict the total deviation and its cumulative effect across multiple scenarios.

To facilitate numerical implementation, the infinite norm and the one-norm can be rewritten in the form of linear inequalities. For the infinite norm constraint, the following formula holds:

$$\|\bar{z_k}\|_\infty \le \gamma_{k,\infty} \iff -\gamma_{k,\infty} 1 \le \bar{z_k} \le \gamma_{k,\infty} 1 \tag{17}$$

For the one-norm constraint, an auxiliary variable $s_k \ge 0$ is introduced, and:

$$\|\bar{z_k}\|_1 \le \gamma_{k,1} \iff \begin{cases} -s_k \le \bar{z_k} \le s_k, \\ 1^T s_k \le \gamma_{k,1}, \\ s_k \ge 0, \end{cases} \tag{18}$$

The two-norm constraint remains as:

$$\|\bar{z_k}\|_2 \le \gamma_{k,2} \tag{19}$$

Thus, the multiple norm constraints can be given by a combination of linear constraints and second-order cone constraints. To facilitate the clear embedding of these constraints in the modeling implementation, the corresponding steps can be organized into the following algorithm flow.

Algorithm 1 Multi-norm constraint embedding procedure

1: Input: scenario set Ω, deviation mappings $\psi_k^{(\omega)}(\cdot)$, thresholds $\gamma_{k,1},\gamma_{k,2},\gamma_{k,\infty}$, number of deviation types K.

2: Initialize decision variables $x(\omega)$ for all $\omega \in \Omega$.

3: For each $\omega \in \Omega$ and each k=1,…,K, compute

$$z_k^{(\omega)} = \psi_k^{(\omega)}\left(x^{(\omega)}\right)$$

4: For each k, stack the deviation vectors as

$$\bar{z_k} = [(z_k^{(1)})T,...,(z_k^{(N_\Omega)}))T]T$$

5: For each kkk, add the 2-norm constraint

$$\|\bar{z_k}\|_2 \le \gamma_{k,2}$$

to the OPF model.

6: For each k, add the ∞-norm bounds

$$-\gamma_{k,1} \le \bar{z_k} \le \gamma_{k,\infty} 1$$

7: For each k, introduce an auxiliary variable sk≥0 and add

$$-sk \le \bar{z}k \le sk,$$

$$1Tsk \le \gamma k,1$$

8: Solve the resulting multi-norm constrained OPF model and obtain the optimal solution.

9: Output: optimal solution that satisfies all multi-norm constraints.

The above algorithm systematically embeds the multi-norm conditions into the optimal power flow model in the order of "construction and concatenation of deviation vectors - addition of 2-norm constraints - addition of equivalent inequalities of infinity norm and one norm constraints", ensuring consistency between the mathematical expression and the numerical implementation.

3.3 The modeling and computational difficulties of multi-norm constraints

After the introduction of multi-norm constraints, the optimal power flow model has undergone significant changes in both structure and scale, bringing a series of difficulties to modeling and solution. These difficulties mainly lie in non-smoothness, dimension expansion, and overall non-convexity [9].

Firstly, the multi-norm itself has non-smooth characteristics. Taking the one-norm and infinity-norm as examples, for a vector $u \in \mathbb{R}_n$, we have:

$$\|u\|_1 = \sum_{i=1}^{n} |u_i|, \quad \|u\|_\infty = \max_{1\le i\le n} |u_i| \tag{20}$$

When some components ui are near zero or multiple components reach the maximum value simultaneously, the above norms are not differentiable at these points and can only be characterized by subgradients. For example, the subgradient set of the one-norm is:

$$\partial\|u\|_1 = \{g \in \mathbb{R}^n : g_i = \begin{cases} \text{sign}(u_i), & u_i \neq 0, \\ [-1,1], & u_i = 0 \end{cases}\} \tag{21}$$

The subgradient of the infinity-norm is related to the set of components that reach the maximum value. This means that in the presence of multi-norm constraints, traditional OPF solvers based on smooth gradients or Newton-type methods are difficult to directly apply and require more complex numerical tools such as subgradients, splitting algorithms, or cone programming solvers [10].

Secondly, multi-norm constraints bring significant dimension expansion after scene stitching. Let the dimension of the k-th class deviation in a single scene be dk, and the number of scenes be N_Ω. Then the dimension of the stitched vector is:

$$z_k \in \mathbb{R}^{d_k N_\Omega} \tag{22}$$

When the equivalent form of the one-norm is introduced, additional variables $s_k \in \mathbb{R}^{d_k N_\Omega}$ and corresponding inequality constraints are needed. The number of new variables and constraints is approximately:

$$N_{\text{var,add}} \approx \sum_{k=1}^{K} d_k N_\Omega, \quad N_{\text{con,add}} = \mathcal{O}(\sum_{k=1}^{K} d_k N_\Omega) \tag{23}$$

When N_Ω is large or the number of deviation types K is large, the model size increases rapidly, and the storage cost and computation time for direct solution will significantly increase. How to control the number of scenes and deviation dimensions while ensuring the effectiveness of multi-norm constraints is an important trade-off in modeling [11].

From the overall structure, although the multi-norm constraints themselves correspond to convex sets, the model remains highly non-convex when coupled with the AC power flow equations [12]. If the multi-norm constraints are incorporated into the objective function in the form of penalty functions, we can obtain:

$$\min_{x} \; f(x) + \sum_{k=1}^{K} \rho_k \, \|\bar{z_k}(x)\|_{p_k} \tag{24}$$

Among them, $\rho_k > 0$ is the penalty coefficient, and $\rho_k \in \{1, 2, \infty\}$. In AC OPF, $\bar{z_k}(x)$ is nonlinearly coupled with voltage phase angles, voltage amplitudes, etc., resulting in both the overall objective and the feasible region being non-convex; if the penalty coefficient ρ_k is too small, the multi-norm constraints will be ineffective; if it is too large, the feasible region may be overly contracted or even have no solution, and at the same time, numerical instability will be exacerbated [13]. Therefore, in the presence of multi-norm constraints, it is necessary to control the model complexity through appropriate approximations (such as scene selection, convex relaxation, or linearization), and avoid excessive conservatism in parameter selection, which is a key difficulty and area for repeated adjustment in mathematical modeling and computational solution.

4 An Improved Mathematical Modeling Scheme for Optimal Power Flow of Power Systems with Multiple Norm Constraints

4.1 The unified extended form of multi-norm couplings

In the modeling of distributed optimal power flow for active distribution networks, the network is typically divided into regions or feeder lines, and each region contains local resources such as distributed power sources, energy storage, and controllable loads. Let the set of regions be $R = \{1,...,R\}$ and the set of scenarios be $\Omega = \{1,...,N\Omega\}$. For each region $r \in R$ and scenario $\omega \in \Omega$, the local decision variables are defined as:

$$x_r^{(\omega)} \in \mathbb{R}^{n_r} \tag{25}$$

and the variables of all regions in the same scenario are concatenated as:

$$x^{(\omega)} = [(x_1^{(\omega)})^T, \dots, (x_R^{(\omega)})^T]^T \tag{26}$$

The operational objective of the active distribution network can be decomposed into a combination of regional local objectives and global performance indicators. Let the local cost of region r in scenario ω be $f_r^{(\omega)}(x_r^{(\omega)})$, then the weighted objective across multiple scenarios is written as:

$$\min_{\{x_r^{(\omega)}\}} \sum_{\omega \in \Omega} \pi_\omega \sum_{r \in \mathcal{R}} f_r^{(\omega)}(x_r^{(\omega)}) \tag{27}$$

Among them, π_ω is the scenario weight. To characterize multiple types of operational deviations such as voltage deviation, branch current margin, and distributed power generation

output fluctuation in the active distribution network, the mapping of the k-th type deviation in the region-scenario dimension is introduced:

$$z_{k,r}^{(\omega)} = \psi_{k,r}^{(\omega)}(x_r^{(\omega)}), r \in \mathcal{R}, \omega \in \Omega \tag{28}$$

For example, voltage deviation mapping, current deviation mapping, or active/reactive power output deviation mapping, etc. All deviation vectors of regions and scenarios are uniformly concatenated as:

$$\widetilde{z_k} = \begin{bmatrix} z_{k,1}^{(1)} \\ \vdots \\ z_{k,R}^{(1)} \\ \vdots \\ z_{k,1}^{(N_\Omega)} \\ \vdots \\ z_{k,R}^{(N_\Omega)} \end{bmatrix} \in \mathbb{R}^{d_k} \tag{29}$$

Among them, d_k is the total dimension of the k-th type deviation. Thus, $\widetilde{z_k}$ simultaneously reflects the coupled deviation characteristics of "multiple regions - multiple scenarios".

The unified feasible set of multi-norm coupling is defined as:

$$\mathcal{Z}_k = \bigcap_{p \in \mathcal{P}_k} \{u \in \mathbb{R}^{d_k} : \|u\|_p \le \gamma_{k,p}\} \tag{30}$$

Among them, $\mathcal{P}_k \subseteq \{1,2,\infty\}$ is the norm combination adopted for the k-th type deviation, and $\gamma_{k,p} > 0$ is the corresponding threshold. Thus, the multi-norm coupling constraints can be unified as:

$$\widetilde{z_k} \in \mathcal{Z}_k, k = 1, \dots, K \tag{31}$$

This means that for any deviation type k, its joint deviation across all regions and scenarios must simultaneously satisfy the defined conditions of the selected norm, the two-norm, and the infinity-norm, achieving multi-scale coordinated control of the overall deviation level, the worst deviation, and the cumulative deviation [16].

Embedding the above deviation constraints into the distributed optimal power flow model of the active distribution network, a unified extended form of multi-norm coupling can be obtained:

$$\begin{aligned} \min_{\{x_r^{(\omega)}\}} \quad & \sum_{\omega \in \Omega} \pi_\omega \sum_{r \in \mathcal{R}} f_r^{(\omega)}(x_r^{(\omega)}) \\ \text{s.t.} \quad & \widetilde{z_k}(\{x_r^{(\omega)}\}) \in \mathcal{Z}_k, \quad k = 1, \dots, K \end{aligned} \tag{32}$$

Where the local power flow and operation constraints ensure physical feasibility within the region, the network coupling and consistency constraints maintain the distribution network topology and interface conditions between regions, and the multi-norm set $\mathcal{Z}_k$ uniformly constrains the voltage, current, and output deviations on a global scale, forming the improved

mathematical modeling starting point of the distributed optimal power flow of the active distribution network under multi-norm constraints [18].

4.2 Experimental evaluation indicators and comparative analysis

Under the distributed framework, the multi-norm constrained optimal power flow of the active distribution network can be abstracted as a distributed convex-nonconvex mixed optimization master problem with consistency constraints. For each region $r \in R$ and scenario $\omega \in \Omega$, the local decision variables are denoted as $x_r^{(\omega)}$, and the global consistency variables are denoted as $y^{(\omega)}$ (such as boundary node voltages, tie-line powers, etc.). The master problem can be formulated as:

$$\begin{aligned} \min_{\{x_r^{(\omega)}\},\{y^{(\omega)}\}} \quad & \sum_{\omega\in\Omega} \pi_\omega \sum_{r\in\mathcal{R}} f_r^{(\omega)}\, g(x_r^{(\omega)}) \\ \text{s.t.} \quad & x_r^{(\omega)} \in \mathcal{X}_r^{(\omega)}, r \in \mathcal{R}, \omega \in \Omega, \\ & A_r^{(\omega)} x_r^{(\omega)} - B_r^{(\omega)} y^{(\omega)} = 0, r \in \mathcal{R}, \omega \in \Omega, \\ & \widetilde{z_k}(\{x_r^{(\omega)}\}) \in \mathcal{Z}_k, k = 1, \dots, K \end{aligned} \tag{33}$$

Among them, $x_r^{(\omega)}$ is the feasible region of local power flow and operation constraints for region r in scenario ω, the matrix $A_r^{(\omega)}$, $B_r^{(\omega)}$ describe the matching relationship between regional boundary quantities and consistency variables, and the multi-norm constraint set $\mathcal{Z}_k$ is defined as in the previous text.

To solve the above master problem under the distributed condition, consistency-constrained Lagrange multipliers $\lambda_r^{(\omega)}$ and penalty parameter $\rho > 0$ are introduced. The augmented Lagrangian function can be written as:

$$\begin{aligned} & \mathcal{L}_\rho(\{x_r^{(\omega)}\},\{y^{(\omega)}\},\{\lambda_r^{(\omega)}\}) = \\ & \sum_{\omega\in\Omega}\sum_{r\in\mathcal{R}} \pi_\omega\, f_r^{(\omega)}(x_r^{(\omega)}) + \sum_{\omega\in\Omega}\sum_{r\in\mathcal{R}} (\lambda_r^{(\omega)})^{\mathrm{T}} (A_r^{(\omega)} x_r^{(\omega)} - B_r^{(\omega)} y^{(\omega)}) + \\ & \frac{\rho}{2} \sum_{\omega\in\Omega}\sum_{r\in\mathcal{R}} \left\| A_r^{(\omega)} x_r^{(\omega)} - B_r^{(\omega)} y^{(\omega)} \right\|_2^2 \end{aligned} \tag{34}$$

Under the condition of satisfying the multi-norm constraints $\widetilde{z_k} \in Z_k$, an alternating update strategy of ADMM type can be adopted:

Region sub-problem update:

$$x_r^{(\omega)} \in \mathcal{X}_r^{(\omega)}, r \in \mathcal{R}, \omega \in \Omega \tag{35}$$

Global consistency variable update:

$$A_r^{(\omega)} x_r^{(\omega)} - B_r^{(\omega)} y^{(\omega)} = 0, r \in \mathcal{R}, \omega \in \Omega \tag{36}$$

Multiplier update:

$$\lambda_r^{(\omega),t+1} = \lambda_r^{(\omega),t} + \rho(A_r^{(\omega)} x_r^{(\omega),t+1} - B_r^{(\omega)} y^{(\omega),t+1}) \tag{37}$$

In practical implementation, for the region sub-problem, a heuristic simplification method can be further utilized to alleviate the non-smoothness and high-dimension burden brought by

the multi-norm structure, and the iteration termination conditions can be set based on the original residual and dual residual:

$$r^{(\omega),t} = A_r^{(\omega)} x_r^{(\omega),t} - B_r^{(\omega)} y^{(\omega),t} \tag{38}$$

$$s^{(\omega),t} = \rho B_r^{(\omega)T} (y^{(\omega),t} - y^{(\omega),t-1}) \tag{39}$$

to ensure obtaining an approximate optimal solution under the condition that both multi-norm constraints and consistency constraints are acceptable.

4.3 The decomposition modeling strategy for power grid zoning

The distributed solution of the active distribution network multi-norm constrained optimal power flow relies on a reasonable grid partition strategy [19]. The distribution network topology is regarded as an undirected graph $G = (N, L)$, where N is the set of nodes and L is the set of branches. It is divided into several subgraphs $G_r = (\mathcal{N}_r, L_r)$, $r \in R$, satisfying:

$$\bigcup_{r \in \mathcal{R}} \mathcal{N}_r = \mathcal{N}, \mathcal{N}_r \cap \mathcal{N}_s = \emptyset, \quad r \neq s \tag{40}$$

The tie-line set is defined as:

$$\mathcal{L}_{tie} = \{(i, j) \in \mathcal{L} : i \in \mathcal{N}_r, j \in \mathcal{N}_s, r \neq s\} \tag{41}$$

Within region r, the local optimal power flow sub-problem under scenario ω can be written as:

$$\begin{aligned} \min_{x_r^{(\omega)}} \quad & f_r^{(\omega)}(x_r^{(\omega)}) \\ \text{s.t.} \quad & g_r^{(\omega)}(x_r^{(\omega)}) = 0, \\ & h_r^{(\omega)}(x_r^{(\omega)}) \leq 0, \\ & C_r^{(\omega)} x_r^{(\omega)} = \xi_r^{(\omega)} \end{aligned} \tag{42}$$

Among them, $g_r^{(\omega)}$ is the power flow balance constraint within the region, $h_r^{(\omega)}$ is the operation constraints such as voltage, current, distributed power sources, energy storage, active and reactive power output, etc.; matrix $C_r^{(\omega)}$ extracts the boundary node voltages and tie-line powers from $x_r^{(\omega)}$, and $\xi_r^{(\omega)}$ represents the corresponding consistency variable. The coupling across regions can be described by consistency constraints. For a tie-line $(i, j) \in \mathcal{L}_{tie}(i, j)$, if nodes i and j belong to regions r and s respectively, then global variables $V_i^{(\omega)}$, $V_j^{(\omega)}$, $P_{ij}^{(\omega)}$, etc. can be introduced to make:

$$V_{i,r}^{(\omega)} = V_i^{(\omega)}, V_{j,s}^{(\omega)} = V_j^{(\omega)} \tag{43}$$

$$P_{ij,r}^{(\omega)} = P_{ij}^{(\omega)}, P_{ji,s}^{(\omega)} = -P_{ij}^{(\omega)} \tag{44}$$

By unifying the $\{V^{(\omega)}, P^{(\omega)}\}$ with the above consistency relations, the physical consistency of voltage and power distribution throughout the active distribution network can be maintained

while ensuring the relative independence of the problems within each region. The multi-norm deviation vector $\widetilde{z_k}$ is constructed by concatenating the deviation vectors $\widetilde{z_V}$,r(ω) of all regions on the region-scenario two-layer, for example, stacking all voltage deviation vectors $\widetilde{z_v}$, r(ω) of the regions as:

$$\widetilde{z_V} = \begin{bmatrix} z_{V,1}^{(1)} \\ \vdots \\ z_{V,R}^{(1)} \\ \vdots \\ z_{V,1}^{(N_\Omega)} \\ \vdots \\ z_{V,R}^{(N_\Omega)} \end{bmatrix} \tag{45}$$

and applying one, two, or infinity norm constraints from the multi-norm set ZV to it, thereby achieving multi-scale coordinated control of the voltage deviation throughout the entire network based on the partition modeling.

4.4 Heuristic modeling and simplification based on multi-norm structure

Although multi-norm constraints help to precisely depict the voltage, current, and output deviation of the active distribution network, they introduce non-smooth terms and significantly increase the model dimension when concatenated in multiple scenarios and regions [20]. In this section, based on the aforementioned unified modeling, we provide heuristic simplification ideas from three perspectives: soft penalty, threshold conversion, and approximate smoothing.

Firstly, some norm constraints of deviation types can be relaxed from hard constraints to soft penalties, while retaining only the hard constraints of key safety indicators. For example, the infinity norm constraint of the terminal node voltage can be maintained as a hard constraint, while writing the one-norm deviation of the line current into the objective function:

$$\min_{\{x_r^{(\omega)}\}} \sum_{\omega\in\Omega} \pi_\omega \sum_{r\in\mathcal{R}} f_r^{(\omega)}(x_r^{(\omega)}) + \sum_{k\in\mathcal{K}_{soft}} \eta_k \left\| \widetilde{z_k}(\{x_r^{(\omega)}\}) \right\|_{p_k} \tag{46}$$

Among them, Ksoft is the set of soft penalty deviation types, $\eta_k > 0$ is the penalty coefficient, and $p_k \in \{1, 2, \infty\}$ is the selected norm. By adjusting ηk, a trade-off can be made between safety margin and economy without explicitly introducing a large number of additional constraints.

Then, simplification can be achieved by using the relationship between different norms. In the case of $u \in R_n^u$, there is:

$$\|u\|_2 \le \|u\|_1 \le \sqrt{n}\,\|u\|_2, \|u\|_\infty \le \|u\|_2 \le \sqrt{n}\,\|u\|_\infty \tag{47}$$

When using the two-norm constraint as the main one, $\gamma_{k,2}$ can be given first, and the following can be adopted:

$$\gamma_{k,1} = \sqrt{d_k}\,\gamma_{k,2}, \gamma_{k,\infty} = \frac{1}{\sqrt{d_k}}\,\gamma_{k,2} \tag{48}$$

Link the one-norm and infinity-norm thresholds with the two-norm, so that in the parameter adjustment stage, only $\gamma_{k,2}$ can be mainly adjusted to indirectly control the other norm constraints, simplifying the threshold design.

Again, the weighted two-norm can be used to approximate the one-norm, converting the non-smooth term into a smooth quadratic term. Let the weight vector of the k-class deviation in the t-th iteration be wk(t), then:

$$\sum_{i} w_{k,i}^{(t)} (\widetilde{z_{k,i}})^2 \tag{49}$$

Approximate $\| \widetilde{z_k} \| 1 = \sum i|\widetilde{z_{k,i}}|$, and update in the iteration:

$$w_{k,i}^{(t+1)} = \frac{1}{\|\widetilde{z_{k,i}^{(t)}}\| + \epsilon} \tag{50}$$

Among them, $\epsilon > 0$ is a constant to prevent division by zero. This weighted strategy can simulate the "sparsity promotion" effect of the one-norm when the deviation tends to be sparse distribution, while maintaining the smoothness and convex quadratic structure of each sub-problem, facilitating the use of mature quadratic programming or second-order cone programming solvers.

With the above heuristic cooperation, although multi-norm constraints still retain the multi-scale control ability of deviations, the dimension and non-smoothness in the actual solution process have been alleviated, providing a more friendly problem structure for the convergence and computational efficiency of distributed solving algorithms.

4.5 Formalization of the multi-norm constrained modeling process

In order to facilitate the reuse of the multi-norm constrained distributed optimal power flow model in different active distribution network engineering scenarios, it is necessary to systematically and formally organize the overall modeling process. Let R be the set of regions, be the set of scenarios, and $K = \{1, \ldots, K\}$ be the set of deviation types. Here, some deviations are in the hard constraint set Khard, and some are in the soft penalty set Ksoft. The overall model can be summarized as:

$$\begin{aligned} \min_{\{x_r^{(\omega)}\},\{y^{(\omega)}\}} \quad & \sum_{\omega\in\Omega} \pi_\omega \sum_{r\in\mathcal{R}} f_r^{(\omega)}(x_r^{(\omega)}) + ' \sum_{k\in\mathcal{K}_{soft}} \eta_k \|\widetilde{z_k}(\{x_r^{(\omega)}\})\|_{p_k} \\ \text{s.t.} \quad & x_r^{(\omega)} \in \mathcal{X}_r^{(\omega)}, r \in \mathcal{R}, \omega \in \Omega, \\ & A_r^{(\omega)} x_r^{(\omega)} - B_r^{(\omega)} y^{(\omega)} = 0, r \in \mathcal{R}, \omega \in \Omega, \\ & \widetilde{z_k}(\{x_r^{(\omega)}\}) \in \mathcal{Z}_k, k \in \mathcal{K}_{hard} \end{aligned} \tag{51}$$

Among them, $p_k \in \{1,2,\infty\}$ is the norm type selected for each type of soft penalty deviation, $\eta_k > 0$ is the corresponding penalty coefficient, and Z_k is the feasible set defined by the intersection of multiple norms.

Based on the above unified expression, the process of multi-norm constrained modeling and assembly can be formally characterized using the following algorithm.

Algorithm 2 Multi-norm constrained D-OPF modeling workflow

1: Input: network topology data, load and DG scenarios (set Ω), partition set R, deviation types K, norm selections p_k, thresholds $\gamma_{k,p}$, and penalty coefficients η_k.

2: Partition the active distribution network into regions r∈R based on topology, feeder structure and DG/ESS locations, and identify tie-lines and boundary nodes.

3: For each region r and each scenario ω, define local decision variables $x_r^{(\omega)}$ and feasible sets $x_r^{(\omega)}$ including power flow equations, operational limits and device-specific constraints.

4: Construct consensus variables $y^{(\omega)}$ and coupling matrices $A_r^{(\omega)}$,$B_r^{(\omega)}$, to represent voltage and power-flow consistency across regions.

5: For each deviation type $k \in K$, define deviation mappings

$$Z_{k,r}^{(\omega)} = \psi k, r(\omega)(x_r^{(\omega)})$$

and stack them into global deviation vectors z~k over all regions and scenarios.

6: For hard-constrained deviations $k \in K_{hard}$, define multi-norm feasible sets

$$Z_k = \cap p \in P_k\{u \in R_d^k : \| u \|_p \leq \gamma_{k,p}\}$$

and add constraints $\widetilde{z_k} \in Z_k$ to the model.

7: For soft-constrained deviations k∈K_{soft}, add penalty terms

$$\eta_k \| \widetilde{z_k} \|_{p_k}$$

to the objective function, with initial choices of ηk based on engineering experience or preliminary sensitivity analysis.

8: Assemble the full D-OPF model according to the unified formulation, combining local feasibility, consensus constraints and multi-norm conditions.

9: Select an appropriate solver or decomposition scheme (e.g, ADMM-based distributed method), and specify stopping criteria using primal and dual residuals as well as multi-norm constraint satisfaction.

10: Run the solver, optionally updating ηk or γk,p if persistent violations are observed, and iterate until convergence.

11: Output: a multi-norm constrained dispatch and voltage profile for the active distribution network over all scenarios, together with deviation indicators for further analysis.

Through the above process, the modeling of the active distribution network multi-norm constrained distributed optimal power flow has formed a reusable operation path from "network and scenario input", "area and deviation type definition", "construction of multi-norm set" to "solver selection and parameter adjustment", and has also provided a unified mathematical basis for the subsequent numerical examples to conduct comparative analysis of different norm combinations, threshold configurations and partition strategies.

5 Numerical examples and result analysis

5.1 Testing system and simulation settings

In order to verify the effectiveness of the distributed optimal power flow modeling method for active distribution networks under multi-norm constraints, numerical examples selected a typical medium-voltage distribution network as the research object, and on this basis, additional active components such as distributed power sources, energy storage devices, and adjustable loads were added. The test scenarios include the renovated IEEE 33-node and IEEE 69-node distribution networks, both of which are radial structures, facilitating the demonstration of the

characteristics of active distribution networks such as longer feeder lengths and sensitive terminal voltages. The basic parameters of the system and the configuration of active components are shown in Table 1.

Table 1: Basic parameters of the tested active distribution network system

System ID	Number of buses	Number of branches	Rated voltage / kV	Base capacity / MVA	DG installed capacity / MW	Energy storage capacity / MW	Maximum active load / MW	Proportion of adjustable load / %
Sys-33	33	32	12.66	10	3.0 (PV-dominated)	1.0	3.7	25
Sys-69	69	68	12.66	10	5.5 (PV + wind power combined)	2.0	5.8	30

Based on the above basic network, typical daily load curves and renewable energy output curves are selected to construct simulation scenarios. The load side is divided into three categories: residential, industrial and commercial, and public loads. Various load states such as "morning rush hour, midday trough, evening rush hour" and "weekend flat peak" are generated through different time period amplification coefficients. The distributed power side considers the output of photovoltaic power under sunny, cloudy and partly cloudy conditions, as well as the changes in wind power output caused by wind speed fluctuations. By comprehensively considering the combination of load and output, twenty representative scenarios are generated, each corresponding to one or several typical periods during the day, and their occurrence probabilities are obtained from historical operation data and normalized.

To better reflect the actual operation of the active distribution network, in the scenario construction, two types of operating conditions with high and low renewable penetration are explicitly distinguished: the former corresponds to large-scale photovoltaic power generation during the noon period and some loads at a medium level, while the latter corresponds to low photovoltaic output at night or during rainy weather and relatively concentrated loads. The multi-norm constraints are mainly applied to key operational quantities such as node voltage deviation, line current margin and distributed power output fluctuations. Considering that the voltage at the end nodes of the distribution network is relatively weak, in this calculation example, different thresholds are set for the overall level of voltage deviation, the maximum deviation of a single node, and the cumulative deviation of multiple scenarios, to be used for subsequent comparison of the changes in voltage quality and line safety margin under different combination of norms.

In terms of regional division, the 33-node system is naturally divided into 3 regions by the main line and branch lines, and the 69-node system is divided into 4 regions. Each region independently conducts power flow calculation and control variable optimization, and couples the power flow of the transmission line and the voltage of the boundary node with adjacent regions. This can not only reflect the engineering habit of the active distribution network's zone operation, but also provide a clear structural basis for subsequent distributed solution algorithms.

5.2 Model implementation and parameter settings

To verify the robustness of the proposed mechanism, we At the implementation level, this paper deploys the distributed optimal power flow model of the active distribution network under multi-norm constraints on a single-machine multi-process simulation platform. The computing environment is: 64-bit Windows operating system, 12-core CPU, 32 GB memory; the algorithm

is written in Python, and each regional sub-problem is solved by calling a commercial second-order cone programming solver; the distributed coordination part is implemented based on the ADMM approach. Considering the engineering reproducibility, all examples are run in the same hardware and software environment without separately enabling parallel acceleration, so as to facilitate the comparison of the impact of different norm combinations and parameter settings on the computing time.

To ensure the stability of numerical solution and the interpretability of the results, the penalty parameters, residual thresholds, maximum iteration steps of the ADMM algorithm, as well as the key parameters of multi-norm constraints and penalty terms have been uniformly set, and are summarized as Table 2.

Table 2: Model Implementation and Main Parameter Setting

Parameter category	Parameter name	Typical value or range	Description
Computing environment	Hardware configuration	12-core CPU, 32 GB RAM	All test cases are run in the same physical environment.
	Software platform	Windows + Python + commercial solver	Local subproblems are solved as second-order cone programs using a commercial solver.
ADMM-related settings	Penalty parameter	10 (tuned in the range 5–20)	Controls convergence speed and numerical stability.
	Maximum number of iterations	300	If exceeded, the case is regarded as hard to converge under the current parameters.
	Primal residual tolerance	1×10^{-4}	Measures how well the inter-area consensus constraints are satisfied.
	Dual residual tolerance	1×10^{-4}	Measures the convergence of the updates of consensus variables.
	Initial multipliers	Zero vector	Facilitates observation of the convergence process.
Multi-norm constraints (voltage deviation)	2-norm threshold	0.08 p.u.	Controls the overall level of voltage deviations.
	Infinity-norm threshold	0.05 p.u.	Limits the maximum voltage deviation at any single bus.
	1-norm threshold or equivalent control coefficient	Scaled by number of buses and the 2-norm threshold	Controls accumulated deviations over multiple buses and scenarios.
	Lower bound of line loading safety margin	0.8	When exceeded, penalties or hard constraints are triggered.
	1-norm penalty coefficient	10	Suppresses long-term high loading of lines.
Penalty terms and weights	Voltage deviation penalty weight	5–20	Larger values place more emphasis on voltage quality.
	Loss and power-purchase cost weight	1 (baseline)	Kept at the same order of magnitude as economic indicators.
	Renewable curtailment penalty	30–50	Higher weight encourages priority use of renewable energy by

	weight		penalizing curtailment.

Based on this, the main program iterates in a "scene - region" dual loop: the outer loop traverses all typical scenarios, and the inner loop conducts ADMM coordination among different regions. In each iteration, all sub-problems in each region are solved in parallel first, and then the boundary voltages and line power flows are updated at the coordination layer. The iteration of each scenario ends when both the original residual and the dual residual are simultaneously below the set threshold, and the number of iterations and the calculation time are recorded for subsequent drawing of the "calculation time - scene convergence ratio" curve.

The calibration of multi-norm-related parameters is carried out in a way of "first providing the acceptable voltage and current deviation range in engineering, and then deducing the threshold": Firstly, the allowable deviation of node voltage and the upper limit of emergency load rate of lines are given by the operation regulations. Then, the two-norm and infinity-norm thresholds are adjusted through small-scale trial calculations to make them just approach the safety boundary in the extreme conditions without multi-norm penalties. On this basis, the one-norm threshold is gradually tightened or the one-norm penalty coefficient is increased to make the voltage profile and line load more balanced in the spatial and temporal dimensions. The obtained set of parameters not only conforms to engineering experience but also lays a unified benchmark for subsequent comparison of the changes in operation indicators under different norm combinations.

5.3 Comparison of results under different parameter combinations

Based on the aforementioned multi-norm constrained optimal power flow model and example settings, in this section, three representative norm combinations are selected for comparison: Scheme A only considers the two-norm constraint, which is used to control the overall deviation level; Scheme B adds the infinite-norm constraint on the basis of Scheme A, which is used to limit the maximum deviation in the worst scenario; Scheme C simultaneously introduces the two-norm, infinite-norm and one-norm constraints, and depicts the overall level, extreme values and cumulative effects of deviations in multiple scenarios through multiple dimensions. To investigate the influence of different norm combinations on the system operation status, simulations are conducted on two example systems, Sys-33 and Sys-69, and the changes in node voltage distribution and operating indicators in different scenarios are plotted, as shown in Figures 1-4.

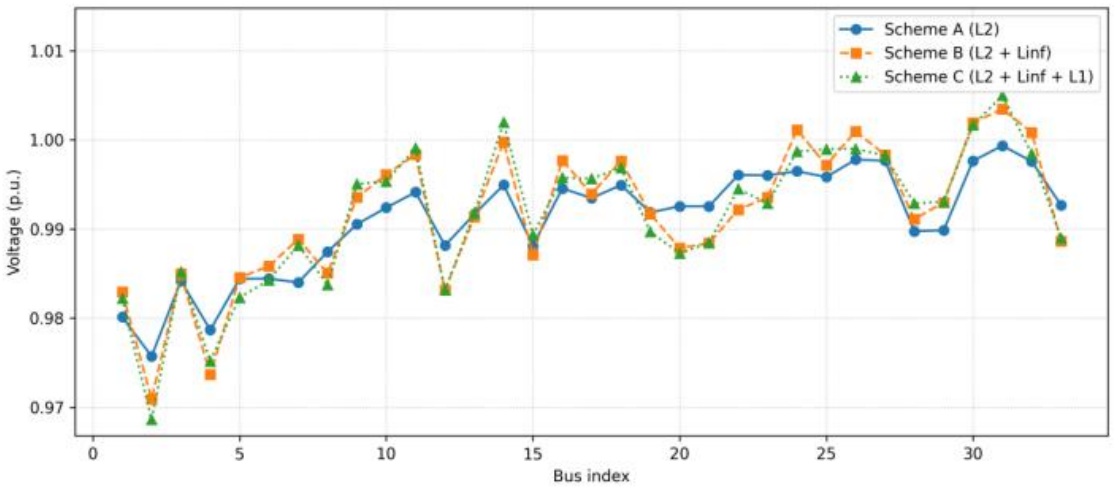

Figure 1: Voltage Curve of Sys-33 Node

From Figure 1, it can be seen that in the Sys-33 system, the voltage curves corresponding to the three schemes have similar overall shapes, but there are significant differences at the terminal nodes and those with concentrated loads. The voltage curve of Scheme A has a certain "concave" shape at these nodes, with local voltage approaching the lower limit; the curve of Scheme B shifts upward overall, and the lowest voltage is somewhat elevated; the curve of Scheme C is the smoothest, and the voltage at the terminal nodes has improved significantly, with the voltage distribution more concentrated in the middle position of the allowable range. This indicates that when only constraining the overall deviation, the system is prone to having a few extreme scenarios or local areas with low voltage. However, after adding the infinite norm and one norm constraints, the model will actively suppress this "a few scenarios are very bad" unbalanced state.

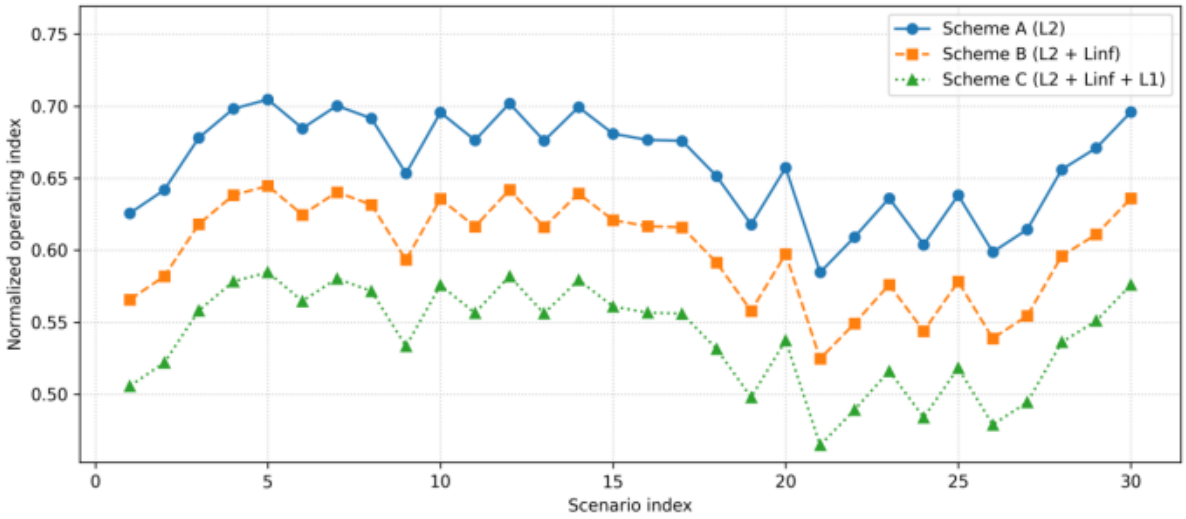

Figure 2: Sys-33 Scenarios-based Operating Indicators Curve

Figure 2 presents the changes of the normalized operating indicators of the Sys-33 system in multiple scenarios with the sequence number of the scenarios. It can be seen that the curve of Scheme A is generally at a high level, with significant peaks and valleys, indicating that in some scenarios, voltage deviation and line overload are still prominent; Scheme B, although still fluctuating in some scenarios, has a significantly lower overall level; Scheme C's curve shifts downward overall and has a smaller fluctuation range. The indicator values in most scenarios remain in a lower range, indicating that the multi-scenario combination constraints can, while ensuring overall feasibility, further improve the balance among different operating scenarios and reduce the concentration of operational risks over time.

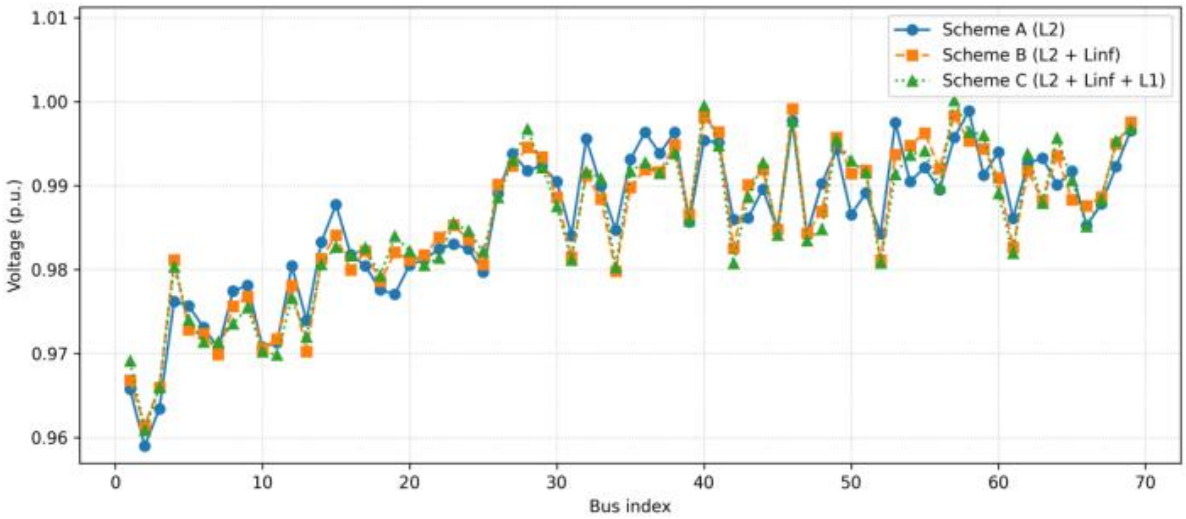

Figure 3: Voltage Curve of Sys-69 Node

For larger-scale Sys-69 systems, the voltage distribution shown in Figure 3 is more distinct. Due to the longer system feeders and more concentrated end loads, under Scheme A, the voltages of some remote nodes are significantly lower than those in the central area, and the voltage curve shows a large spatial gradient; under Scheme B, the curve rises overall, and the number of low-voltage nodes decreases; in Scheme C, the voltage curve becomes significantly smoother in the end area, and the local "peaks" or "valleys" are weakened, indicating that the multi-norm constraints have a more prominent improvement effect on the voltage quality in complex networks.

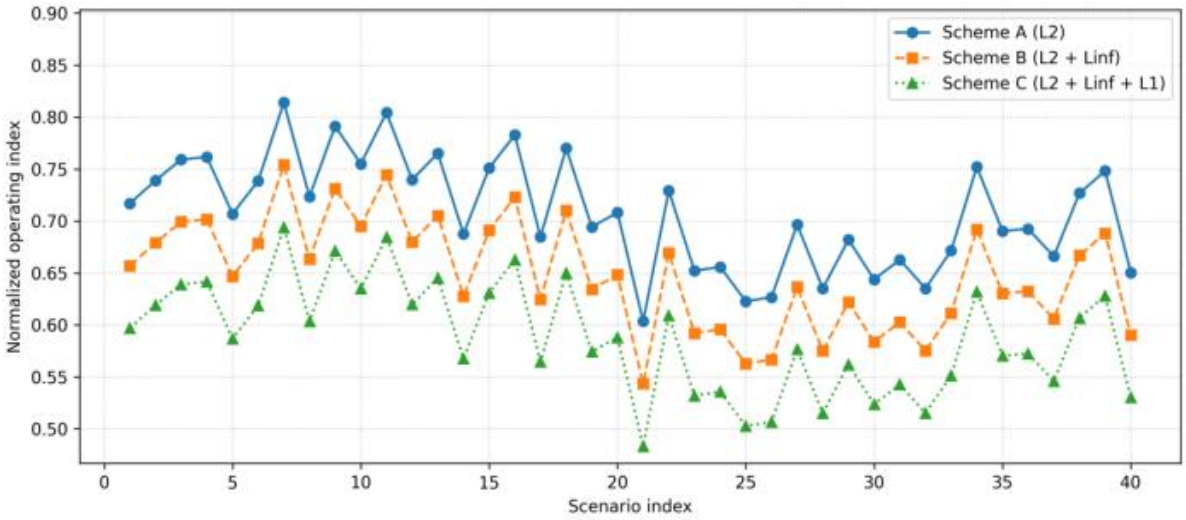

Figure 4: Sys-69 Scenarios-based Operating Performance Curve

Figure 4 illustrates the normalized operating performance indicators of the Sys-69 system in different scenarios. Overall, the relative positions of the three curves are similar to those of the Sys-33 system: Scheme A consistently remains at the highest level, and in some scenarios, it shows significant peaks; the Scheme B curve shifts downward overall, with a reduction in the number and height of peaks; the Scheme C curve is at the bottom and has the most stable fluctuations, with the indicator values of most scenarios concentrated in a lower range. This

result indicates that when the number of nodes and branches significantly increases, relying solely on the two-norm constraint is difficult to simultaneously ensure the operation quality of all scenarios, while the multi-norm combination can more effectively compress the risk level of "long-tail scenarios" and enable the system to maintain a relatively consistent and acceptable operating state across a wider range of scenarios.

By comparing Figures 1-4 comprehensively, it can be seen that as the norm combination gradually expands from a single two-norm to "two-norm + infinity-norm + one-norm", both test systems exhibit a trend of evolving from "dispersed, unbalanced" to "concentrated, stable" in terms of node voltage distribution, inter-scenario indicator fluctuations, and extreme scenario control. It should be noted that although Scheme C performs best in terms of voltage quality and operation risk, compared to Scheme A and Scheme B, it also requires more reactive power regulation capabilities and certain active power losses. Therefore, in practical engineering applications, the multi-norm combination does not have an absolute "optimal" status; instead, it provides a parameter configuration path for dispatchers to make trade-off choices between safety margin, economy, and operational balance.

5.4 Analysis of the Impact of Multiple Norm Constraints on Operating Indicators

In the aforementioned example, the multi-norm constraints are characterized by the two-norm for the overall deviation level, by the infinity-norm for extreme scenario deviations, and by the one-norm to reflect the cumulative effect of deviations in each scenario. To further investigate the impact of norm thresholds and weight settings on the system's operational performance, this section conducts multiple rounds of scans on the comprehensive operational indicators under different parameter combinations, and analyzes the optimization results from multiple perspectives such as "indicator variation amplitude, norm term contribution structure, and residual distribution".

Figure 5 presents the volcano plot of the influence of multi-norm parameter perturbations on the comprehensive operational indicators. The horizontal axis represents the variation of operational indicators relative to the benchmark scheme, and the vertical axis represents the statistical significance of the corresponding variation (represented by $-\log_{10}(p)$). The light-colored dots near the zero point in the figure represent most of the small-amplitude parameter adjustments, which have limited improvement or deterioration on the comprehensive indicators; while the dark-colored triangular points distributed on both sides and significantly elevated vertically correspond to the significant decrease or increase in the voltage overrun ratio, line overload times, and comprehensive indicators of active power network loss when the L_2 threshold, $L\infty$ threshold, and L_1 weight undergo significant changes.

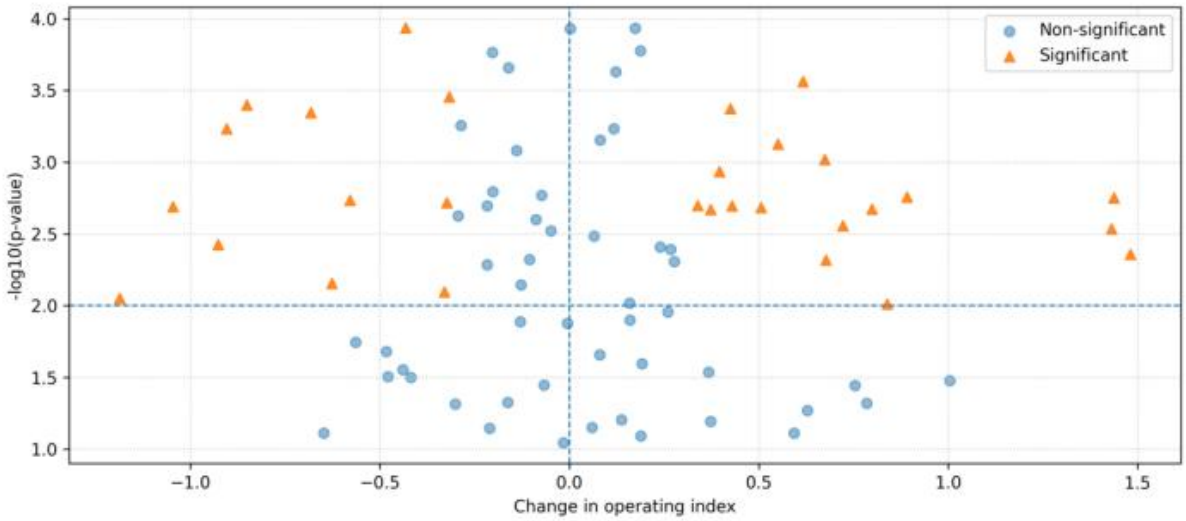

Figure 5: Volcano plot showing the impact of multi-norm parameter perturbations on the overall operational indicators

As can be seen from the figure, in the area where the $L\infty$ threshold is moderately tightened and the L_1 weight is increased, a cluster of "significant and highly effective" points gathers in the upper right corner, indicating that by strengthening the constraints on extreme scenarios and cumulative deviations, a significant reduction in operational risks can be achieved to a certain extent; when the three types of norm constraints are simultaneously relaxed, a small number of significant points also appear in the upper left corner, corresponding to the risk intervals where the comprehensive indicators deteriorate significantly. This provides an intuitive "unfavorable region" indication for parameter tuning.

Figure 6 shows the contribution structure of each norm term to the overall constraint intensity under different norm threshold scaling factors. The x-axis represents the norm threshold scaling factor changing from 0.8 to 1.2, and the y-axis represents the percentage contribution of L_2, $L\infty$, and L_1 norm constraints in the total constraint intensity.

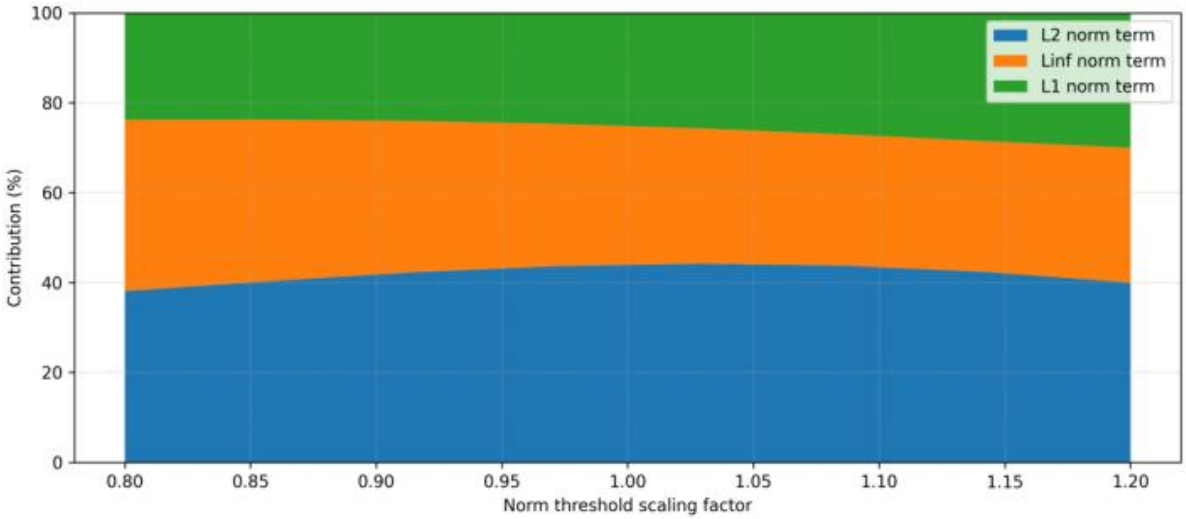

Figure 6: Percentage cumulative area chart of the contribution of each norm constraint under different threshold scaling factors

As shown in Figure 6, when the scaling factor is small, the contribution of the infinity norm constraint significantly increases, indicating that the model is more focused on compressing the maximum deviation and controlling the most unfavorable scenarios. As the threshold gradually relaxes, the proportion of the two-norm constraint gradually rises. The model measures the operating status more through the overall mean square deviation, while the contribution of the one-norm constraint remains relatively stable within different scaling intervals, mainly undertaking the balanced adjustment role for moderate deviation scenarios. The percentage cumulative area chart intuitively reflects the structural division of labor between multiple norm combinations in "preventing extreme scenarios" and "considering the overall level", providing a basis for subsequent targeted adjustments of each norm threshold and weights according to engineering requirements.

To evaluate the stability of the multi-norm model in fitting the operating indicators, Figure 7 presents a heat map of the residual distribution under different scenarios and threshold scaling combinations. The x-axis represents the scenario number, and the y-axis represents the scaling factor of the norm threshold. The color intensity corresponds to the size of the residual of the comprehensive operating indicators.

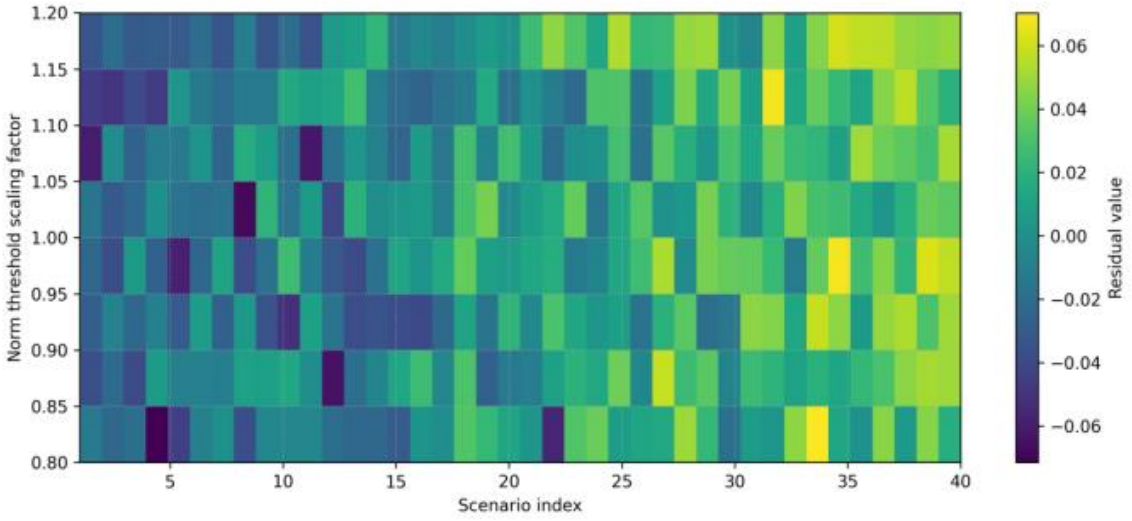

Figure 7: Heat map of the residual distribution under multi-norm constraints

Overall, the residuals are concentrated in relatively small intervals in most areas, and only in the vicinity of the areas with high load and voltage tension do scattered darker bands appear, indicating that the model has a smaller fitting error in most normal operating conditions, and only in a few extreme combinations does there exist a slightly larger deviation. Compared with the volcano chart in Figure 5, it can be found that these regions with larger deviations often correspond to parameter settings with relatively loose norm constraints and insufficient control over tail scenarios, which from a side perspective confirms the role of multi-norm combinations in suppressing operational risks under extreme conditions.

Figure 8 presents the L_2 norm threshold scaling factor, $L\infty$ norm threshold scaling factor, and comprehensive operation indicators in the same coordinate system in the form of a three-dimensional scatter plot. The horizontal and vertical coordinates are the scaling factors of L_2 and $L\infty$, and the height of the vertical axis represents the size of the comprehensive operation indicators.

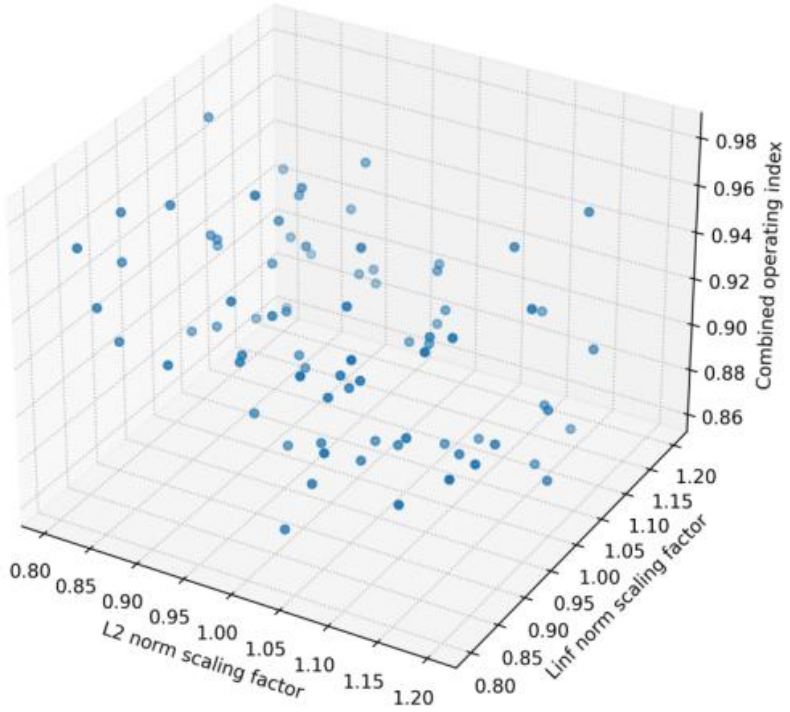

Figure 8: Three-dimensional scatter plot of the comprehensive operation indicators under different combinations of L_2 and $L\infty$ thresholds

From Figure 8, it can be observed that the point cloud shows a trend of gradually moving upward as the L_2 and $L\infty$ thresholds increase. When both types of norm thresholds are relatively large, the comprehensive operation indicators deteriorate significantly, indicating that overly relaxing the constraints on overall deviation and maximum deviation will cause voltage over-limit and line overload to reappear in several scenarios. However, within the combination range of L_2 and $L\infty$ thresholds that are relatively small or one is larger and the other is smaller, the scatter points have significantly lower heights and are more densely distributed, reflecting a more balanced trade-off between safety margin and economy in the operating state. The three-dimensional view provides the approximate distribution of the "acceptable area" and "high-risk area" of multi-norm combinations in the L_2–$L\infty$ plane from the perspective of the parameter space, which is beneficial for dispatchers to prioritize selecting parameter combinations near the low-index "valley" during engineering setting.

Based on the analysis of Figures 5 to 8, multi-norm constraints not only change the sensitivity of operation indicators to different types of deviations by adjusting the relative weights and thresholds of the three types of norm terms, but also form a relatively clear "safety-economy" trade-off boundary in the parameter space. Reasonable selection of the combination of L_2, $L\infty$, and L_1 can not only significantly reduce risk indicators such as voltage over-limit and line overload, but also maintain the stability of model fitting and the acceptability of residual distribution, providing a visual-supported decision-making basis for optimal power flow parameter setting in multiple scenarios and complex conditions.

6 Conclusion

This paper is aimed at the multi-scenario operation of the active distribution network. It proposes a distributed OPF model with multi-norm constraints to uniformly describe the overall

deviation, single-node extremum, and multi-scenario cumulative deviation. It also provides a modeling process that can be used for regional-scenario decomposition and solution. The simulation is based on the modified IEEE 33 and 69-node distribution networks, with DG configured at 3.0/5.5 MW, energy storage at 1.0/2.0 MW, and maximum active load at 3.7/5.8 MW. 20 typical load-output scenarios are constructed, and voltage two-norm thresholds of 0.08 p.u., infinity-norm threshold of 0.05 p.u., and line load safety lower limit of 0.8 are set for comparison. The results show that under the above configuration, the multi-norm combination can significantly raise the voltage at the end nodes, reduce the scenarios of line overload, and smooth the multi-scenario operation index curves. This provides a quantitative and visual reference for parameter tuning in the active distribution network between safety and economy.

About the Author

Maolin Sheng was born in Lu'an, Anhui, China, in 1979.He is currently working at Anhui Electrical Engineering Professional and Technical College.His research interests focus on applied mathematics

References

[1] Sultan Hassan Hakmi, Hashim Alnami, Badr M. Al Faiya & Ghareeb Moustafa.(2025). Multidimensional Optimal Power Flow with Voltage Profile Enhancement in Electrical Systems via Honey Badger Algorithm. Biomimetics, 10(12), 836-836. https://doi.org/10.3390/BIOMIMETICS10120836.

[2] Ramdhan Halid Siregar,Akhyar Akhyar,Rakhmad Syafutra Lubis & Muhammad Nurul Hadi.(2025).Optimal Power Flow-Assisted Unit Commitment with Multi-Level Load Variation Analysis in Renewable-Based Power Systems.Energies,18(23),6340-6340. https://doi.org/10.3390/EN18236340.

[3] Lei Zhang.(2025).The Present Study Investigates the Coordinated Optimisation of Optimal Power Flow and Economic Dispatch in Power Systems based on Intelligent Optimisation Algorithms.International Journal of Energy,7(3),5-13. https://doi.org/10.54097/Z13W8E29.

[4] Mohamed A.M. Shaheen,Hany M. Hasanien,Ibrahim Alsaleh,Abdullah Alassaf,Miao Zhang & Ayoob Alateeq.(2025).Optimal power flow in power systems with renewable energy resources uncertainty including geothermal power plants.Ain Shams Engineering Journal,16(12),103784-103784.https://doi.org/10.1016/J.ASEJ.2025.103784.

[5] Shuning Zhou.(2025).Deep Reinforcement Learning Based Distributed Optimization Framework for Optimal Power Flow in Multi-Region Power Systems.Journal of Electrical Engineering & Technology,20(8),1-12.https://doi.org/10.1007/S42835-025-02362-8.

[6] Xiaochen Zhang,Kaijie Xu,Shengchen Liao,Lin Qiu,Chengjin Ye & Youtong Fang.(2025).Disturbed security-constrained and time-variant optimal power flow for dynamic power system based on chaotic-genetic-centroid puffin optimization.Applied Energy,397,126287-126287.https://doi.org/10.1016/J.APENERGY.2025.126287.

[7] Priya E. & Preetha Roselyn J. (2025).An integrated approach for multi-objective differential algorithm based event constrained optimal power flow for power system resiliency enhancement.Sustainable and Resilient Infrastructure, 10(4), 351-370. https://doi.org/10.1080/23789689.2024.2414140.

[8] Xiaoyuan Luo,Weisong Zhu,Xinyu Wang & Xinping Guan.(2025).Optimal Power Flow Scheduling for All-electric Ship Power System based on Improved Whale Algorithm.Smart Grids and Sustainable Energy,10(2),43-43. https://doi.org/10.1007/S40866-025-00267-Z.

[9] Xiaoqiang Wei,Jiayi Wang,Xinyan Cui,Shilong Li & Hao Yang.(2025).Optimal Power Flow Control of Synchronous Generators for Short Circuit Ratio Enhancement in Power Systems with High-Proportion Wind Power Level.Journal of Physics: Conference Series,3012(1),012047-012047.https://doi.org/10.1088/1742-6596/3012/1/012047.

[10] Xin Dong, Wenjuan Du, Qiang Fu & Haifeng Wang.(2025).Domain-adversarial graph neural network for small-signal stability constrained optimal power flow in AC/DC renewable power systems.Electric Power Systems Research,247,111775-111775. https://doi.org/10.1016/J.EPSR.2025.111775.

[11] Haewon Byeon,Wajdi Alghamdi,Munni Evin,M. Sucharitha,D. David Neels Ponkumar,A. Prakash & J. Sunil.(2025).A novel swarm intelligence-based approach for solving optimal power flow problems in modern power systems.Results in Control and Optimization,19,100555-100555.https://doi.org/10.1016/J.RICO.2025.100555.

[12] Amin Besharatiyan,Saeid Jowkar,Ali Esmaeel Nezhad,Ehsan Rahimi,Fariba Esmaeilnezhad, Toktam Tavakkoli Sabour... & Ayda Demir.(2025).Tackling optimal power flow in modern power systems using a new optimization strategy.Frontiers of Engineering Management,12(4),1-22.https://doi.org/10.1007/S42524-025-4167-2.

[13] Liangcai Zhou,Long Huo,Linlin Liu,Hao Xu,Rui Chen & Xin Chen.(2025).Optimal Power Flow for High Spatial and Temporal Resolution Power Systems with High Renewable Energy Penetration Using Multi-Agent Deep Reinforcement Learning. Energies,18(7),1809-1809.https://doi.org/10.3390/EN18071809.

[14] Fahad Alsokhiry.(2024).Leveraging Harris Hawks Optimization for Enhanced Multi-Objective Optimal Power Flow in Complex Power Systems. Energies, 18(1), 18-18. https://doi.org/10.3390/EN18010018.

[15] Mokhtar Abid,Messaoud Belazzoug,Souhil Mouassa,Abdallah Chanane & Francisco Jurado.(2024).Optimal power flow of thermal-wind-solar power system using enhanced Kepler optimization algorithm: Case study of a large-scale practical power system.Wind Engineering,48(5),708-739.https://doi.org/10.1177/0309524X241229206.

[16] Ebeed Mohamed,Abdelmotaleb Mohamed A.,Khan Noor Habib,Jamal Raheela,Kamel Salah,Hussien Abdelazim G.... & Sayed Khairy.(2024).A Modified Artificial Hummingbird Algorithm for solving optimal power flow problem in power systems.Energy Reports,11,982-1005.https://doi.org/10.1016/J.EGYR.2023.12.053.

[17] Saeed Badoozadeh, Nazila Nikdel, Sadjad Galvani & Mohammad FarhadiKangarlu.

(2023). Probabilistic optimal power flow in wind energy integrated power system based on the K-medoids data clustering method considering correlated uncertain variables.IET Renewable Power Generation,17(13),3179-3194.https://doi.org/10.1049/RPG2.12834.

[18] Dulău Lucian Ioan & Bică Dorin.(2022).Optimal Power Flow Analysis of a Power System with Distributed Generators and Storage Considering Seasons.Tehnički vjesnik,29(6),1819-1826.https://doi.org/10.17559/TV-20210723100305.

[19] Zhu Jun-Hua, Wang Jie-Sheng, Zhang Xing-Yue, Song Hao-Ming & Zhang Zhi-Hao.(2023). Mathematical distribution coyote optimization algorithm with crossover operator to solve optimal power flow problem of power system.Alexandria Engineering Journal,69,585-612.https://doi.org/10.1016/J.AEJ.2023.02.023.

[20] Nguyen Thang Trung,Nguyen Hung Duc & Duong Minh Quan.(2023).Optimal Power Flow Solutions for Power System Considering Electric Market and Renewable Energy.Applied Sciences,13(5),3330-3330.https://doi.org/10.3390/APP13053330.